Macromolecules

pubs.acs.org/Macromolecules Article

Nonlinear Shear and Extensional Rheology of Telechelic Metallosupramolecular Networks

Pierrot de Wergifosse,* Maxime Dalne, Alvaro Quinteros-Sedano, and Evelyne van Ruymbeke

Cite This: *Macromolecules* 2026, 59, 4636−4649 Read Online

ACCESS | Metrics & More | Article Recommendations | Supporting Information

ABSTRACT: We investigate the nonlinear shear and extensional rheology of telechelic metallosupramolecular polymer networks in the melt state. Poly(*n*-butyl acrylate) (P*n*BA) star precursors with varying molecular spans (unentangled, barely entangled, and well-entangled) are end-linked through metal−ligand complexes with varying bond strengths (Zn^{2+}, Cu^{2+}, and mixtures). Linear viscoelastic properties are quantitatively described by using the Rouse model for short stars and a time-marching algorithm tube model for entangled stars. In nonlinear start-up shear, densely cross-linked networks obtained from the association of unentangled precursors exhibit pronounced shear hardening before reaching a maximum when stickers start dissociating. For these systems, a strong failure of the Cox−Merz rule is observed, in contrast to networks based on entangled precursors. In shear, the yielding strain, γ_{max}, is found to be independent of the shear rate when sticker exchange is slow relative to deformation, indicating strain-controlled bond dissociation and an effective nonlinear sticker lifetime scaling as $\tau_{sticker,\ NLVE} \approx \gamma_{max}/\dot{\gamma}$. The maximum stretching ratio is a key parameter to rationalize transient behavior in both shear ($\lambda_{max} \approx N_{strand}^{1/2}$) and elongation ($\epsilon_{H,\ max} \approx \ln N_{strand}^{1/2}$). Entanglements introduce additional dissipation through chain sliding, reducing strain hardening and enhancing network toughness.

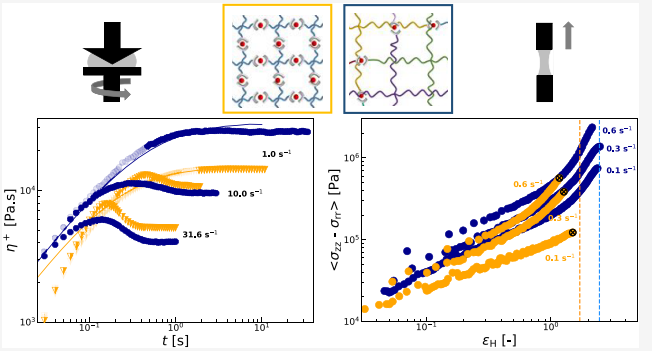

1. INTRODUCTION

Supramolecular polymer networks (SPNs) consist of polymeric precursors connected through reversible physical cross-links ("stickers"). These stickers span a broad range of chemistries — including hydrogen bonds,[1−4] metal−ligand coordination,[5−7] and ionic interactions[8−11]—whose bond strengths can be tuned to control viscoelastic properties,[12] enabling reprocessability,[13,14] energy dissipation,[7,15,16] or self-healing.[3,5,17,18]

The linear viscoelasticity (LVE) of SPNs (melts and gels) has been extensively studied.[19] Sticky Rouse[9] and sticky reptation[20] models accurately describe the relaxation of unentangled and entangled linear chains bearing associating side groups (or stickers) along their backbone. In these models, the molecular strands between two consecutive stickers serve as a new reference unit for the coarse-grained representation of a chain and the slow relaxation process of the transient networks is taken into account by considering the stickers as extra friction points along the chain backbone. By accounting for an overall delay on the relaxation processes due to the stickers dynamics, it is thus possible to describe the viscoelastic properties of these samples while keeping an approach similar to the one used for linear chains.

This framework is, however, not suitable to describe the dynamics of transient polymer networks built from the association of telechelic building blocks with supramolecular moieties only located at their extremities. Indeed, with such networks, the stickers are not uniformly distributed along the chain backbone, and an average influence on each molecular segment cannot be considered anymore. Moreover, their viscoelastic response may strongly vary as a function of the relative importance of their entanglements and sticker lifetimes. While this large tunability is particularly interesting to design physical networks with desired properties, this requires, first, rationalization of the different processes behind the relaxation of these transient networks. As discussed by Boudara et al.,[21] telechelic stars appear as the most convenient architecture to achieve this objective. Considering a star arm to be pinned at one end (branching point), it has only two possible states. In the case of associated stickers, no relaxation is possible. When the sticker dissociates, the star arm can relax through contour length fluctuations.

In ref 22, we studied the LVE behavior of model metallosupramolecular (MS) networks formed from either

Received: February 13, 2026
Revised: March 25, 2026
Accepted: March 27, 2026
Published: April 6, 2026

https://doi.org/10.1021/acs.macromol.6c00463
Macromolecules 2026, 59, 4636−4649

short or long (entangled) telechelic star precursors, to understand the contribution of both stickers and entanglements to the linear dynamics of these SPNs. These systems were found to be thermorheologically complex, as precursor mobility follows Williams−Landel−Ferry (WLF) behavior, whereas sticker exchange follows Arrhenius dynamics. To decouple the two temperature dependencies, pseudomaster curves turned out to be a very useful tool.[9] Based on a modified time-marching algorithm (TMA) tube model, we showed that sticker exchange dynamics share the same temperature dependence across architectures, while the temperature dependence of the terminal regime was found to be strongly affected by the coupling between sticker exchange and arm disentanglement, leading to their own temperature dependence. This coupling could be captured by our model, providing a tool to interpret the linear viscoelastic response of such telechelic networks.

Besides the linear regime, exploring the nonlinear response of SPNs under large shear or elongation remains an open field of research. Recent instrumental advances, such as the cone-partitioned-plate (CPP) geometry[23] for shear and filament stretching rheometers (FSRs)[24] for extensional flows, now enable reliable measurements deep in the nonlinear viscoelastic region (NLVR). Accessing high Weissenberg numbers (Wi) is particularly useful for SPNs, where chain stretching competes directly with sticker dissociation, revealing composition−property relationships inaccessible via LVE alone.

Several nonlinear features of SPNs recurrently appear in experiments, theory, and simulations. Simulation results showed that start-up shear and extensional flows of transient networks built from unentangled telechelic molecules often reveal transient strain hardening at large Wi_c (= $\dot{\gamma}\tau_c$ or $\dot{\epsilon}_H\tau_c$, with τ_c, the terminal relaxation time taken as the inverse crossover frequency between G' and G'').[25−29] Under strong flows, network strands can become strongly oriented and stretched before sticker dissociation allows chain retraction. In particular, simulations (of shear and extensional flows) of associative telechelic chains with strong bond energy by Amin et al.[25] attributed the overshoot above the LVE envelope to non-Gaussian chain stretching (finite extensibility) and reorientation of chain segments along the flow direction.

Experimentally, under elongation flow, an important strain hardening was observed with entangled polymer chains bearing stickers along their backbone when deformed at large Wi. While in ref 30, sticky junctions were formed via hydrogen bonds, strain hardening was obtained thanks to ionic interactions in ref 31. However, there is nearly no data on the elongation properties of telechelic systems. In ref 32, the authors investigated the elongation properties of short telechelic linear polybutadienes end-functionalized with acid groups neutralized with different alkali metal ions. The importance of strain hardening was found to depend on the strength of the supramolecular junctions.

While for simple polymer melts, the steady-state shear viscosity η_{steady} typically matches the complex viscosity obtained from linear oscillatory measurements,[33,34] the failure of the Cox−Merz rule is usually observed with telechelic systems displaying delayed shear thinning[29,35] and possibly shear thickening.[27,28] The importance of these deviations seems to depend on the building block topology, cross-linking density, chain stretching, and possible sticker recombination once they are dissociated. In refs 27,36, the authors investigated the behavior of hydrophobically modified ethoxylated urethane (HEUR) in aqueous solution. They observed transient shear hardening, which was attributed to the flow-induced stretching of the network, followed by its disruption and decrease of the cross-linking density. The influence of the strong dilution (few wt %) of the precursor on the observed behavior is, however, not clear. In ref 37, Pyromali et al. studied the shear properties of transient networks based on entangled telechelic star building blocks. The authors did not observe such transient strain hardening.

Another feature of the nonlinear shear response of transient networks built from telechelic molecules is the yielding strain or the strain at the stress-overshoot maximum (γ_{max}). This is indeed a key parameter for understanding how network rearrangement takes place, what is the stretching state of network strands, and whether the bond dissociation is stress-, strain-, or time-controlled. Some studies report a Wi-dependence of γ_{max},[17,37,38] and others do not,[26,37] emphasizing the need for systematic investigation.

The large diversity of responses of SPNs under fast flows can be attributed to the multiple competing time scales governing their behavior.[8,39,40] Depending on the deformation rate, reversible bonds may behave as dynamic cross-links or, effectively, as permanent junctions when $\dot{\gamma}$ (or $\dot{\epsilon}_H$) exceeds $1/\tau_{sticker}$. Polymer relaxation times further influence possible sticker recombination ($\tau_{sticker}$ vs $\tau_{c,ref}$, with $\tau_{c,ref}$ the terminal relaxation time of a precursor) and thus the amount of energy dissipated before failure, influencing whether SPNs behave in a brittle-like or ductile-like manner.

For example, Arora et al.[39] used high-speed imaging combined with a FSR to map the extensional response of wormlike-micelle networks bridged by telechelics. They identified two regimes for the filaments: continuous thinning (flow) at low Wi and brittle-like fracture (without necking) at high Wi, when the Hencky strain rate roughly exceeds the inverse of the lowest characteristic relaxation time of the system. The observed brittle behavior indicated that energy dissipation processes were not significant in their systems. Yet, looking at the crack-tip profile and by varying the composition (and therefore the connectivity), they found out that dense networks break in the elastic regime, whereas loosely connected networks display important strain hardening before failure occurs.

Using different counterions, Liu et al.[40] were able to fine-tune sticker dynamics in sulfonated polystyrene ionomers based on unentangled precursors. They showed that, at high extension rates, whether the Rouse-like motions of the precursors are sufficiently slow compared to the associative lifetime or not, networks can either achieve ductility (higher energy dissipation) or, on the contrary, may lead to macroscopic failure (brittle behavior), attributed to the important chain retraction taking place once the bonds are dissociated.

Other studies have explored how combining entanglements with reversible bonds enhances energy dissipation. Wu et al.[8] showed that sparsely cross-linked ionomer gels with flexible unentangled precursors can achieve high stretchability. They highlighted a "pseudo-yielding" at the stretching ratio $\lambda_{max} = N_{strand}^{1/2}$, with N_{strand} being the number of Kuhn segments per network strand ($N_{strand} \gg N_{precursor}$). From a mechanical point of view, Kim et al.[41] designed polymer elastomers and gels, where entanglements greatly outnumber (chemical) cross-links, that combine both high modulus and toughness. They showed that, while cross-links prevent disentanglement, when a

https://doi.org/10.1021/acs.macromol.6c00463
Macromolecules 2026, 59, 4636−4649

chain is stretched under external stress, the tension is transmitted along its length and redistributed via entanglements to many neighboring chains, preventing stress concentration and catastrophic brittle failure.

The aim of the present work is to take advantage of our model telechelic star molecules to investigate the influence of their entanglement state, sticker lifetime, and applied flow on their nonlinear responses, both in shear and in elongation. Compared to sticky chains (with stickers along their backbone), telechelic molecules have the great advantage of allowing modulation of the disentanglement time of the arms in a different way than the sticker lifetime. We build on previous nonlinear shear results obtained with entangled precursors (Pyromali et al.[37]) and combine them with new shear and extensional measurements on networks formed from unentangled and barely entangled precursors. This allows us to rationalize the contribution of both stickers and entanglements to the nonlinear viscoelastic properties of MS networks. We investigate the impact of systematic compositional changes on features such as possible sticker recombination, bond lifetime, strain hardening, Cox−Merz behavior, strain at the stress overshoot, and brittle- or ductile-like behavior under strong extensional flows.

Our systems are particularly suited for isolating these effects. We worked in the melt state to avoid solvent effects, used well-defined (low dispersity) telechelic 4-arm poly(*n*-butyl acrylate) (P*n*BA) precursors, with terpyridine chain ends, synthesized by reversible addition−fragmentation chain-transfer (RAFT), and systematically varied arm length (network strand size). P*n*BA is amorphous with a low T_g (∼−50 °C), enabling access to metal−ligand bis-complex dynamics. At the low metal-ion contents used here, bis-complexes do not aggregate.[42] Moreover, varying metal-ion nature allows straightforward tuning of bond strength to analyze its effect on nonlinear viscoelastic properties of short precursors as it was done with the entangled stars.[37]

The manuscript is organized as follows: we first detail, in Section 2, the samples and the experimental methods used in this work. We then present and discuss experimental results in Section 3: linear and nonlinear shear results for star precursors (Section 3.1) and linear and nonlinear shear and elongation results for the MS networks (Section 3.2). We finally draw conclusions in Section 4.

2. MATERIALS AND METHODS

2.1. Materials

Telechelic P*n*BA precursors with terpyridine (tpy) chain ends were synthesized via RAFT polymerization, as detailed in ref 43 and the Supporting Information. A tetrafunctional chain-transfer agent was used to obtain 4-arm stars. The number-average molar mass of the precursors (M_{star}), the number-average molar mass of the star arms (M_{arm}), the molar mass polydispersity ($Đ$), and the glass transition temperature (T_g) are listed in Table 1. As the molecular span M_{span} (weight-average) for *Star35k-ref* and *Star50k-ref* is shorter than $M_c = 2M_e$, with M_e= 18 kg/mol for P*n*BA, these two samples are considered unentangled. On the contrary, *Star250k-ref* is well-entangled, with an average of ∼3.4 entanglements per arm.[42] A scheme of the precursors, along with their chemical structure, is shown in Figure 1.

Star35k-ref and *Star250k-ref* precursors (and the networks based on them) were prepared in the framework of previous studies,[22,37,42,43] while the *Star50k-ref* precursors (and the networks based on them) were synthesized in the framework of this study. Consistently with ref 22, the name "*Star50k-ref*" refers to the weight-average molar mass estimated by GPC, approximately 50 kg/mol. For the latter, a deconvolution of the asymmetric chromatogram (see Figure S2), using M_{arm}= 13 kg/mol (as determined from ^{1}H NMR data), confirms a majority population of 4-arm stars, as it was suggested for *Star35k-ref* in ref 22.

Table 1. Molecular Characteristics of Telechelic P*n*BA Star Precursors

precursor	M_{star} [kg/mol][a,c]	$Đ$ [-][a]	M_{arm} [kg/mol][b,c]	T_g[°C][d]
Star35k-ref	25	1.40	10	−45
Star50k-ref	36	1.28	13	−47
Star250k-ref	249	1.20	62	−50

[a]Determined by gel permeation chromatography (GPC). [b]Determined by proton nuclear magnetic resonance (^{1}H NMR). [c]Number-average molar masses. [d]Determined by differential scanning calorimetry (DSC).

2.1.1. Ion Incorporation. Metal ions (Zn^{2+}, Cu^{2+}, or equimolar blends) were added to the precursors, forming bis-complexes with the tpy ligands. This step resulted in the formation of single or dual MS networks. The network preparation protocol is detailed in ref 22. As shown in Figure 2 and further discussed in the following sections, the prepared MS networks have similar mesh sizes. Depending on the span of the precursors, the mesh size originates either from the molar mass between two stickers (M_{XX}) or from the molecular segments between two entanglements (M_e). No significant change in T_g was observed upon the addition of ions.[22,43]

2.1.2. Nomenclature. The composition of the MS networks is detailed in Table 2. We use a nomenclature consistent with ref 22: The precursor is indicated, followed by the ion nature and finally the ion (M^{2+}) to ligand (tpy) molar ratio, e.g., *Star50k-Cu-0.5* is a MS network with *Star50k-ref* as the precursor, containing one Cu(II) ion for two terpyridine ligands.

2.2. Methods

2.2.1. Linear Shear Measurements. Small-amplitude oscillatory shear (SAOS) measurements were performed using either a stress-controlled MCR-301 rheometer (Anton Paar) or a strain-controlled ARES rheometer (TA Instruments). Approximately 50 mg of the material was loaded between 8 mm diameter parallel plates. Due to the low T_g of P*n*BA (≈−50 °C), preliminary sample shaping was not feasible. Instead, samples were equilibrated in the rheometer, under a nitrogen atmosphere (convection oven), for 30 min at the highest investigated temperature.

The material was then compressed to a gap of ∼0.8 mm to form a discoid sample, and normal force relaxation was checked prior to testing. The linear viscoelastic region (LVR) was determined from preliminary dynamic strain sweeps at each temperature. Dynamic frequency sweeps were conducted between (maximum) 100 °C and (minimum) −25 °C over an angular frequency range of 80 to 0.1 rad/s (logarithmically spaced). Frequency sweeps were repeated to ensure reproducibility.

2.2.2. Nonlinear Shear Measurements. Start-up shear tests were performed on an ARES rheometer equipped with a force rebalance transducer (2KFRTN1), under a nitrogen atmosphere. Tests were conducted at various fixed shear rates ($\dot{\gamma}$) and the shear stress growth coefficient—referred to hereafter as the transient viscoelastic response—$\eta^+(t) = \sigma^+(t)/\dot{\gamma}$, with $\sigma^+(t)$ the transient shear stress, was recorded.

The measuring system consisted of a homemade cone-partitioned-plate geometry that we received from Prof. Dimitris Vlassopoulos (IESL-FORTH, Greece). Its properties has been described in detail in ref 23. Briefly, the bottom element is a standard cone (diameter of 25 mm, cone angle of 0.1 rad, truncation of 53 μm). The upper element comprises an inner measuring plate (diameter 6 mm) and an outer nonmeasuring ring attached to the transducer head. The gap between the inner plate and the outer partition is ≤ 100 μm. The purpose of the outer ring is to hold a sample with a larger radius relative to the measuring inner plate radius. Consecutive measurements were spaced enough to give the samples time to equilibrate. Once entering the

https://doi.org/10.1021/acs.macromol.6c00463
Macromolecules 2026, 59, 4636−4649

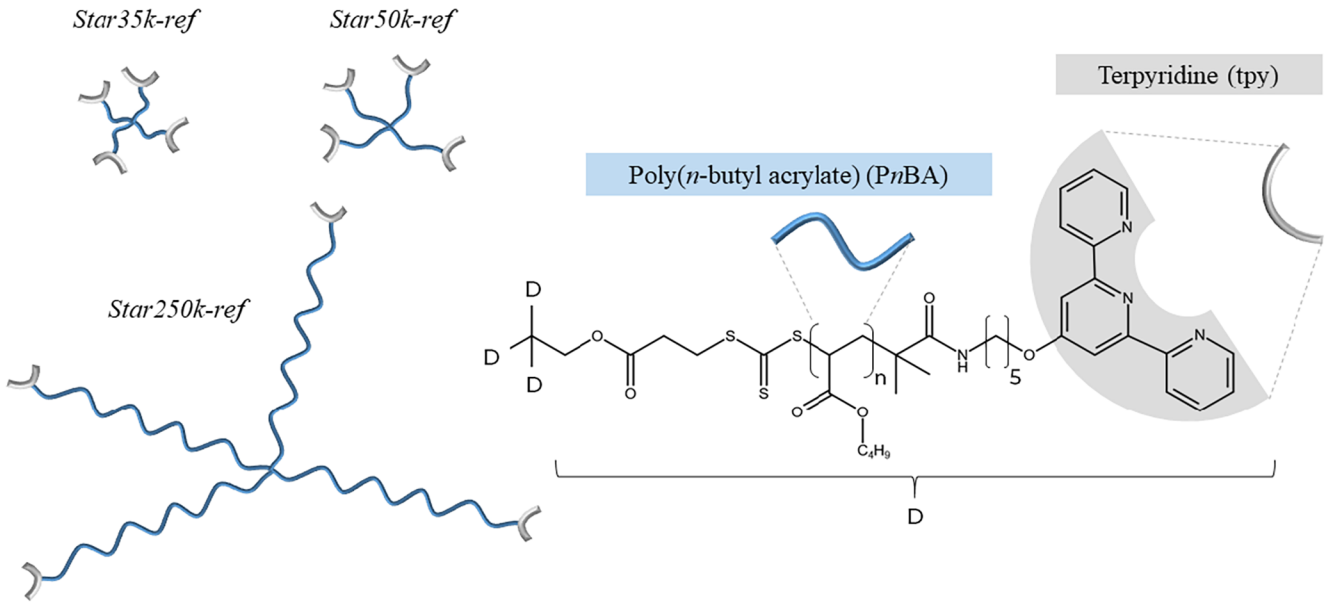

Figure 1. Cartoon and chemical structure of the P*n*BA precursors (4-arm stars with different molar masses).

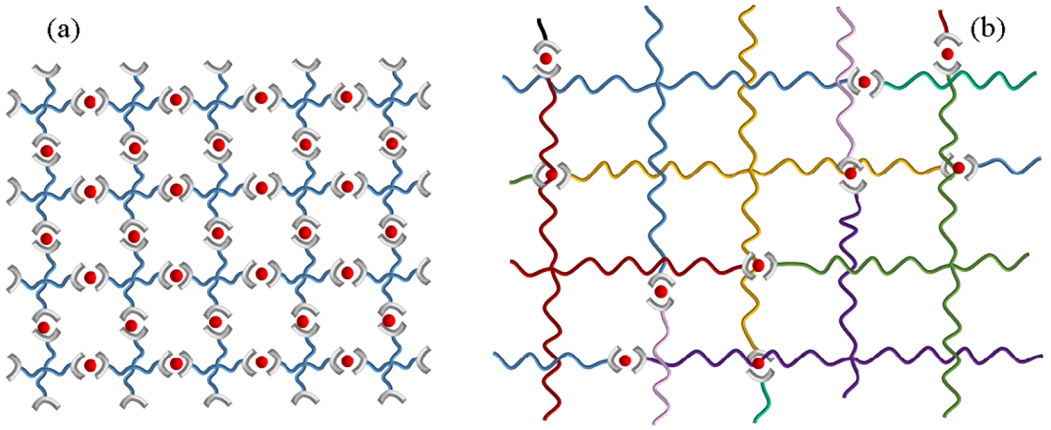

Figure 2. 2D cartoon of two MS networks with similar mesh sizes of two different origins. (a) Using short precursors, the mesh size is dictated by M_{XX}, the molar mass between two branching points. The sticker density is high. (b) Using entangled precursors, the mesh size is dictated by M_e, the molar mass between two entanglements. The sticker density is low.

Table 2. Composition Details of Investigated MS Networks

MS network	ion nature	M^{2+}/tpy ratio [equiv]
Star35k-Zn-0.5	Zn^{2+}	0.5
Star35k-Cu-0.5	Cu^{2+}	0.5
Star35k-ZnCu-0.5	Zn^{2+}/Cu^{2+}	0.25/0.25
Star50k-Zn-0.5	Zn^{2+}	0.5
Star50k-Cu-0.5	Cu^{2+}	0.5
Star50k-ZnCu-0.5	Zn^{2+}/Cu^{2+}	0.25/0.25
Star250k-Zn-1.0	Zn^{2+}	1.0
Star250k-Cu-1.0	Cu^{2+}	1.0
Star250k-ZnCu-1.0	Zn^{2+}/Cu^{2+}	0.5/0.5

NLVR, after every 3−4 increasing shear rates, a measurement at a shear rate in the LVR was performed again to ensure reproducibility and to confirm that no fracture, slip, or shear banding occurred in the inner measuring section.

Two practical limitations were encountered with our systems and with start-up shear measurements in general. First, to preserve the samples, we avoided maintaining strong flows for extended periods. Consequently, steady-state is not always fully reached, although it is closely approached. Second, the shortest precursors exhibit very low viscosity at ambient temperature and tend to flow into the gap between the inner and outer cylinders. These samples must therefore be tested at negative temperatures, which can cause condensation in the rheometer and generate residual normal or torsional forces.

We also note that repeated exposure of MS networks to strong flow fields can induce a higher concentration of M^{2+}/tpy monocomplexes, which—especially for Cu^{2+}—may exhibit an aggregation tendency.[44] This can produce small but measurable changes in the low-shear steady-state viscosity. Given the low ion density in our systems, this effect is considered negligible.

2.2.3. Uniaxial Elongational Measurements. Start-up uniaxial elongation tests were performed on a VADER 1000 filament stretching rheometer.[24] Experiments were conducted, under an ambient air atmosphere, at various fixed Hencky strain rates ($\dot{\epsilon}_H$), recording the elongational stress growth coefficient, $\eta_E^+(t) = \langle \sigma_{zz} - \sigma_{rr} \rangle / \dot{\epsilon}_H$, where $\langle \sigma_{zz} - \sigma_{rr} \rangle$ is the midheight (transient) stress difference.

The elongation properties of the precursors could not be measured due to their viscosity being too low. MS networks of ∼45 mg were loaded between 6 mm diameter parallel plates. They were first annealed in the rheometer at 100 °C, then pressed, and shaped at 60 °C to reach a height of ∼1.5 mm and a midheight radius of ∼3.1 mm (aspect ratio ≈ 0.48). At the same temperature, samples were

https://doi.org/10.1021/acs.macromol.6c00463
Macromolecules 2026, 59, 4636−4649

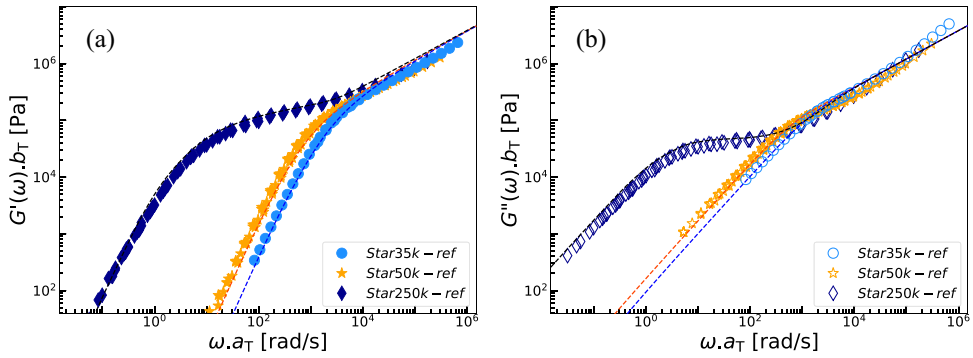

Figure 3. (a) Storage modulus G' and (b) loss modulus G'' for the three P*n*BA star precursors. Master curves built at $T_{ref} = T_g + 75$ °C using the WLF shift factors a_T from ref 22. Dashed lines are the Rouse model predictions for *Star35k-ref* and *Star50k-ref* and the tube-based model predictions for *Star250k-ref*.

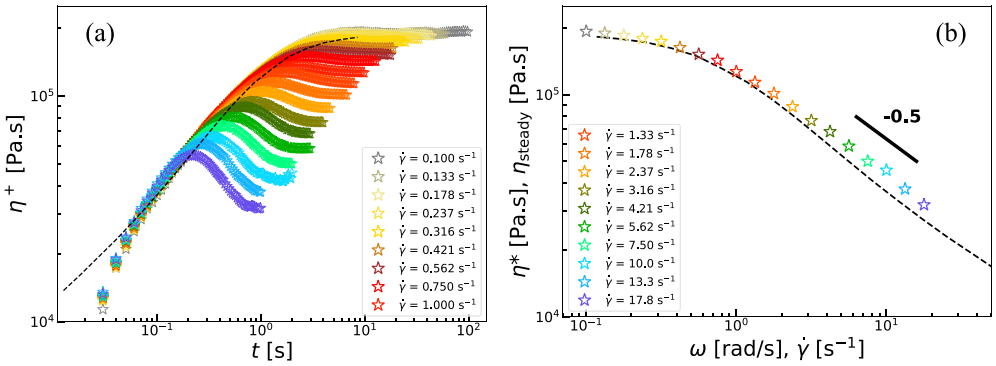

Figure 4. (a) Transient viscoelastic response $\eta^+(t)$ and (b) Cox–Merz representation for the unentangled precursor *Star50k-ref* at $T = -15$ °C. Each color (common legend) corresponds to a start-up shear test performed at a constant shear rate ($\dot{\gamma}$). Dashed lines represent the LVE envelope. The slope at high shear rates is indicated in (b). At −15 °C, $\tau_R \approx 1.96$ s for *Star50k-ref*.

prestretched until the midheight diameter was reduced to 2.8−3.0 mm. The temperature was then lowered to the measurement temperature (40 °C).

During elongational tests, the force was recorded with a load cell, and the midheight diameter was monitored using a laser micrometer. Further details on the FSR setup,[24] the control scheme,[45] and the correction factor accounting for radial variations due to the shear component of the deformation field[46] can be found elsewhere.

3. RESULTS AND DISCUSSION

3.1. Precursors

3.1.1. Linear Viscoelasticity. Figure 3 presents the storage (G') and loss (G'') moduli for the three precursors (Table 1). Master curves were constructed using WLF horizontal shift factors a_T with parameters $C_1 = 6.2$[-], $C_2 = 131.17$ K at $T_{ref} = T_g + 75$ °C,[22] and vertical shift factors b_T to account for the variation of the monomeric density with temperature, $b_T = \rho_{ref} T_{ref}/\rho T$, following ref 47. *Star250k-ref* is well-entangled, showing a clear plateau prior to terminal relaxation, in good agreement with tube-based predictions for monodisperse entangled stars using the following parameters: $G_N^0 = 160$ kPa, $M_e = 18$ kg/mol, and $\tau_e = 5.94 \times 10^{-4}$ s. The TMA tube model used for the predictions is described in detail in ref 22.

The two shortest precursors display a Rouse-like relaxation. As expected, *Star50k-ref*, which has a longer (barely entangled) molecular span compared to *Star35k-ref*, exhibits a longer relaxation time. This is captured by comparison with the Rouse model.[48] We approximate the relaxation of short star polymers by that of linear chains with molar mass M_{span} equal to twice M_{arm} and a reduced dispersity $Đ$ (eq S1). The stress-relaxation modulus is

$$G_R(t) = \frac{\rho RT}{M_{span}} \sum_{p=1}^{N_{span}} \exp\left(-\frac{2p^2 t}{\tau_R}\right) \quad (1)$$

where N_{span} is the number of Kuhn segments along the span, R the gas constant, and τ_R the Rouse time associated with M_{span}.

For *Star35k-ref*, we use a linear analogue with $M_n = 16$ kg/mol and $Đ = 1.2$; for *Star50k-ref*, $M_n = 28$ kg/mol and $Đ = 1.14$. Both corresponding weight-average molar masses lie below the critical entanglement molar mass $M_c = 2M_e$, confirming that these precursors are effectively unentangled. At $T_{ref} = T_g + 75$ °C, the resulting Rouse times are 0.68 ms for *Star35k-ref* and 1.87 ms for *Star50k-ref*. The imperfect high-frequency agreement arises from glassy modes near T_g, which are not captured by the model.

3.1.2. Nonlinear Viscoelasticity. Start-up shear measurements on the precursor *Star250k-ref* were previously reported by Pyromali et al.[37] and are not repeated here. As discussed in Section 2, the transient viscoelastic response of *Star35k-ref* could not be measured in our lab, except at very low shear rates, while our colleagues from IESL-FORTH could obtain data at slightly higher shear rates (see Figure S13). On the contrary, the shear properties of *Star50k-ref* could be measured on a whole range of shear rates and data are shown in Figure 4. Its behavior is representative of that of unentangled stars.

Figure 4a shows the transient viscoelastic response of *Star50k-ref* at −15 °C together with the linear viscoelastic envelope. The latter was constructed from oscillatory tests in

https://doi.org/10.1021/acs.macromol.6c00463
Macromolecules 2026, 59, 4636−4649

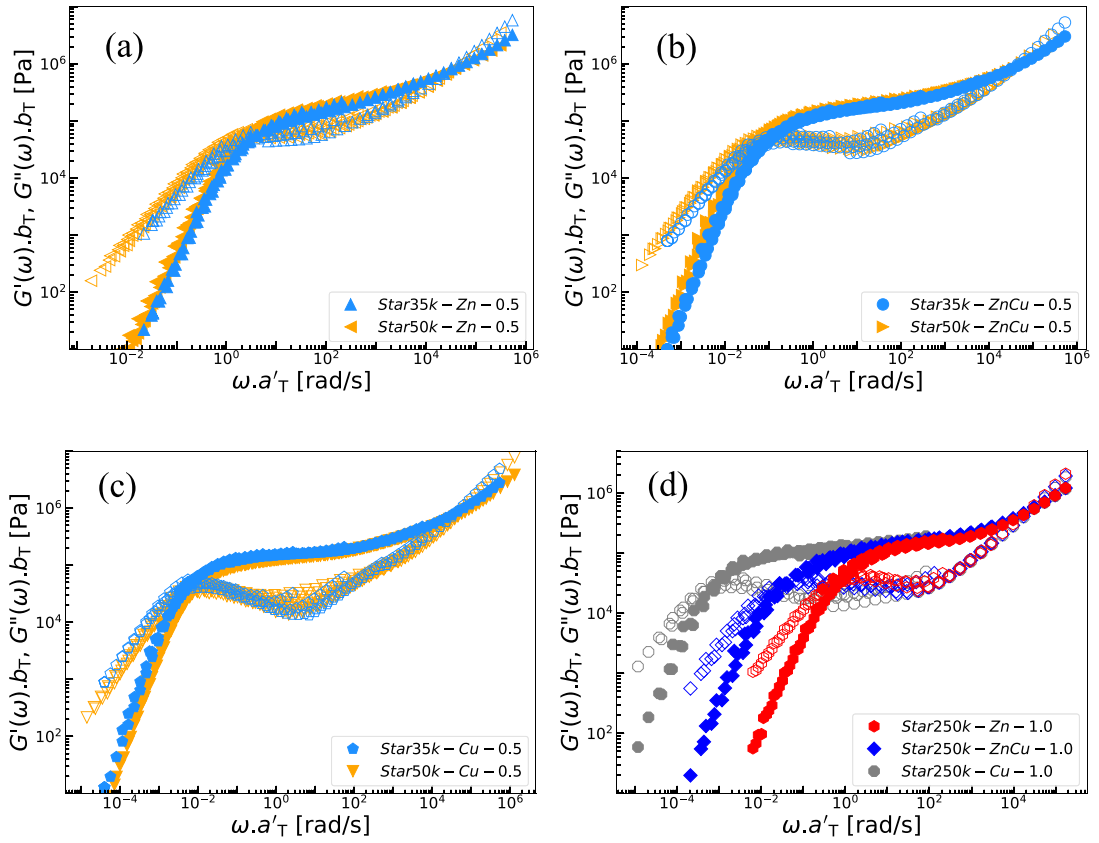

Figure 5. (a–c) Pairwise comparison of G' (full symbols) and G'' (empty symbols) for MS networks built from *Star35k-ref* or *Star50k-ref*. Ion content: (a) 0.5 equiv. Zn^{2+}; (b) 0.25 equiv. Zn^{2+}/0.25 equiv. Cu^{2+}; and (c) 0.5 equiv. Cu^{2+}. Pseudomaster curves built at $T_{ref} = T_g + 75$ °C using the shift factors a'_T, combining WLF and Arrhenius shifts, from ref 22. The activation energies E_a used for the shifts are (a) 40 kJ/mol, (b) 57.5 kJ/mol, and (c) 75 kJ/mol. (d) Pseudomaster curves for MS networks built from *Star250k-ref* with activations energies from left to right: 60 kJ/mol, 40 kJ/mol, and 20 kJ/mol as in ref 22.

the LVE regime (Figure 3) using the Gleissle rule ($\eta^+_{LVE}(t) \approx \eta^*(\omega)|_{\omega=1/t}$).[49] The corresponding frequency sweep and measured shear rate window are shown in Figure S3. The $\dot{\gamma}$ range spans both the LVR and NLVR while avoiding the glassy regime, where G' and G'' diverge at high ω. The Cox–Merz representation,[33] comparing complex viscosity (LVE) and steady-state viscosities obtained from start-up experiments, is shown in Figure 4b.

In Figure 4a, a deviation is observed below $t \approx 50$ ms because the motor requires ~ 0.1 s to reach constant angular velocity; $\eta^+(t)$ is therefore underestimated before this time.[50] At low shear rates, relaxation is fast enough compared to the flow, to ensure that all Rouse modes equilibrate across the molecular span,[50] so $\eta^+(t)$ matches the LVE envelope. At higher shear rates, the $\eta^+(t)$ curves fall below the LVE envelope and display an overshoot before reaching a steady-state value. This behavior begins at $\dot{\gamma} \approx 0.316$ s^{-1}, slightly below $\dot{\gamma} \approx 1/\tau_R(T = -15$ °C$) \approx 0.51$ s^{-1}, likely due to the branching point, which is not captured by the Rouse model. As $\dot{\gamma}$ increases, the η_{steady} decreases (shear thinning, see Figure 4b), while the overshoot amplitude grows. Such trends are well-known and have also been reported for other polymer melts: linear[50,51] or branched.[34,52−55]

Within the explored shear rate range, the overshoot relaxes monotonically to the steady state, with no clear undershoots, as reported for unentangled linear chains under high shear rates.[25,50,51] While at high shear rates, the data must be considered with care as the steady-state regime is only just reached, these data suggest that the presence of a branching point reduces arm alignment along the flow, limiting tumbling or chain overstretching before reaching η_{steady}.[34,56,57]

The Cox–Merz representation in Figure 4b shows good agreement between LVE and steady-state viscosities ($\eta_{steady}(\dot{\gamma}) \approx \eta^*(\omega)|_{\omega=\dot{\gamma}}$).[33] At the highest shear rates, a slight deviation appears, as also noted by other authors.[58,59] It may partly originate from the experimental limitations at strong flows. At high shear rates, a shear dependence of $\eta_{steady}(\dot{\gamma}) \propto \dot{\gamma}^{-1/2}$ is observed, consistently with the shear behavior of unentangled linear chains. As detailed in ref 50, this thinning exponent is well-explained by the shear slit model, according to which, the molecules are confined by the flow in the velocity gradient direction, with a confinement length scale equal to the size of a shear strand of mass M_s, with M_s fixed to ensure that its Rouse time is $\tau_R(M_s) = 1/\dot{\gamma}$.

3.2. Metallosupramolecular Networks

3.2.1. Linear Viscoelasticity. In a previous publication,[22] using a modified TMA tube model, we showed that sticker exchange dynamics (activation energy) in MS networks are independent of the size of the star precursors (*Star35k-ref* vs *Star250k-ref*), whereas the influence of temperature on terminal relaxation is not; a lower effective activation energy was found for the entangled *Star250k-ref*, based on the temperature dependence of its terminal relaxation.

Pseudomaster curves built for all of the samples from Table 2 are shown in Figure 5. The activation energies used to horizontally shift the data are indicated in legend, while the

https://doi.org/10.1021/acs.macromol.6c00463
Macromolecules 2026, 59, 4636−4649

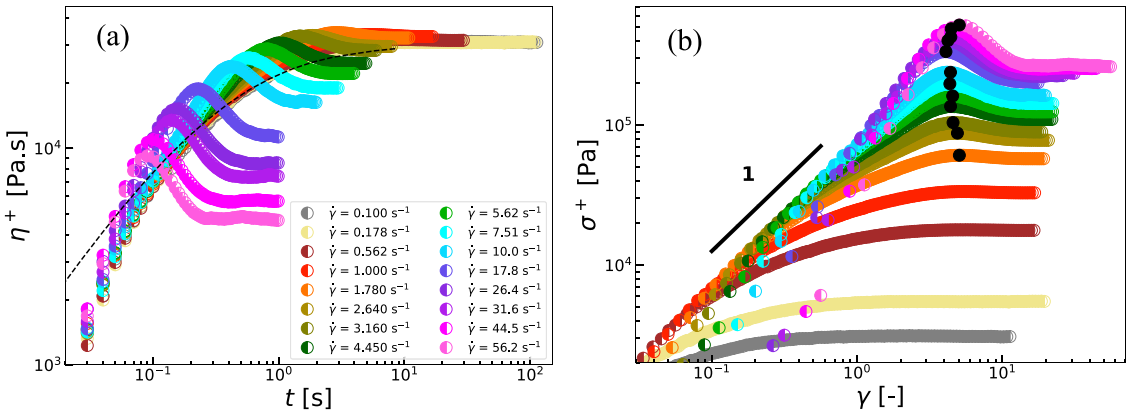

Figure 6. NLVE shear properties of a MS network: *Star35k-ZnCu-0.5*, at T = 40 °C. (a) Transient viscoelastic response $\eta^+(t)$. The black dashed line represents the LVE envelope. (b) Stress−strain representation of the same data. Black symbols indicate the maximum of each curve having a significant overshoot, at coordinates (γ_{max}; σ^+_{max}). The $\dot{\gamma}$ legend in (a) is common with (b).

shifting method involving both WLF and Arrhenius horizontal shift factors can be found in our previous publication[22] and in the SI.

In our former work,[22] it was also concluded that for MS networks based on the unentangled *Star35k-ref* precursors, the activation energy for terminal relaxation matches that of sticker exchange. This observation is further validated in Figure 5a−c, which compare MS networks formed from *Star35k-ref* or *Star50k-ref* precursors with 0.5 equiv of M^{2+} (Zn^{2+}, Zn^{2+}/Cu^{2+}, or Cu^{2+}).

In all three of the first subfigures, the same activation energy was used for both unentangled samples. It is observed that the data nearly overlap, which suggests that the terminal relaxation time is governed solely by sticker dynamics, independent of sticker density (higher for *Star35k-ref*) or precursor span (higher for *Star50k-ref*). Nevertheless, while these transient networks have the same terminal regime, one could expect small differences in their rubbery plateau. This is not observed here because the larger span molar mass of *Star50k-ref* is probably compensated by the presence of a few entanglements along the assemblies created from this precursor (M_{span} close to $2M_e$).

In a more general way, all MS networks in this study (Table 2) exhibit similar plateau moduli (~160 kPa), consistent with comparable mesh sizes, although the origin of the latter differs with the precursor size (Figure 2). For *Star35k-ref*-based networks, the plateau modulus mainly reflects the molar mass between branching points (M_{XX} ≈ 20 kg/mol). For *Star250k-ref*-based networks, it rather reflects the molar mass between entanglements for P*n*BA (M_e = 18 kg/mol). *Star50k-ref*-based networks are an intermediate case for which the plateau modulus reflects M_{XX} (≈26 kg/mol) with an additional elastic contribution from a few entanglements.

At certain temperatures, the MS networks (entangled or not) can display similar LVE spectra, with terminal relaxation times of similar magnitude. Comparing such systems provides an efficient way to isolate compositional effects under fast flows, a strategy previously applied to branched vs linear polymers[52,60] and to melts vs solutions.[51] We follow the same approach in the next subsection to assess the roles of the ion nature and precursor size.

3.2.2. Nonlinear Viscoelasticity: Start-Up Shear. *3.2.2.1. Influence of Stickers and Their Nature.* To illustrate the impact of ion incorporation on the NLVE properties of unentangled precursors, Figure 6 shows the start-up shear response of one representative MS network, *Star35k-ZnCu-0.5*. Full results for MS networks based on unentangled precursors (*Star35k-ref* and *Star50k-ref*) are provided in Figures S4−S10.

Figure 6a presents the transient viscoelastic response of *Star35k-ZnCu-0.5* at 40 °C together with its LVE envelope. The corresponding frequency sweep and measured shear rate window are shown in Figure S11. Figure 6b shows the same data plotted as shear stress ($\sigma^+ = \eta^+(t)\,\dot{\gamma}$) versus strain ($\gamma = t\,\dot{\gamma}$); the overshoot maxima (γ_{max}; σ^+_{max}) are highlighted with black symbols.

At low shear rates (within the LVR), the transient viscoelastic response follows the LVE envelope. At higher shear rates, however, *Star35k-ZnCu-0.5* shows pronounced transient shear hardening. The transient viscoelastic response overshoots well above the LVE envelope before decreasing to its steady-state value, where shear thinning remains present. When the flow is fast relative to network rearrangement, M^{2+}/tpy bis-complexes behave temporarily as fixed cross-links. The network strands undergo stretching until stickers start to dissociate, after which $\eta^+(t)$ decreases. As with unentangled star precursors, no undershoot is observed.

From Figure 6a and from their linear viscoelastic behavior, we conclude that for MS networks based on unentangled precursors the NLVE response is governed solely by the sticker dynamics. Indeed, at 40 °C, the Rouse time of *Star35k-ref* is ~0.25 ms, so reaching a Rouse Weissenberg number $Wi_R = \dot{\gamma}\tau_R = 1$ would require a shear rate $\dot{\gamma} \approx 4000$ s^{-1}. Hence, the stretching of the arm cannot be attributed to its too slow segmental dynamics.

In contrast, deviations from the LVE envelope begin at $\dot{\gamma} \approx 0.5$ s^{-1} and the transient data display an overshoot above $\dot{\gamma} \approx 2.64$ s^{-1}, corresponding to a terminal Weissenberg number $Wi_c = \dot{\gamma}\tau_c \approx 0.4$. The nonlinear behavior of the network is thus related to the inability of the building blocks to move faster than the flow, with the sticker dynamics being too slow compared to the time scale of the flow, $1/\dot{\gamma}$.

In Figure 4b, it is observed that the transient stress curves first increase with strain, following an initial slope of 1. This reflects the elastic response of the network supported by associated stickers, which act as permanent bonds. Then, at the highest shear rates ($\dot{\gamma}$ > 10 s^{-1}), the stress increase is even more pronounced before the overshoot maximum, which suggests that the network strands become stretched. The

https://doi.org/10.1021/acs.macromol.6c00463
Macromolecules 2026, 59, 4636−4649

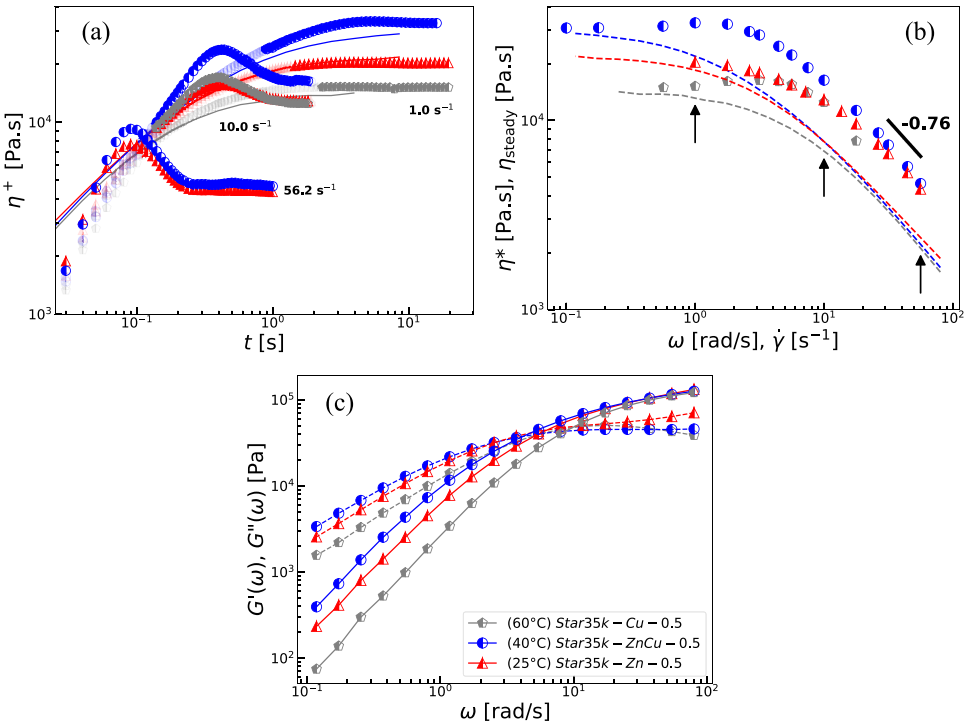

Figure 7. Influence of the ion nature. Comparison of NLVE properties of three MS networks built from *Star35k-ref*. (a) Transient viscoelastic response at three different shear rates. Some data are shaded for clarity. LVE envelopes are indicated by straight lines. (b) Cox–Merz representation. Dashed lines correspond to the LVE envelopes. Black arrows indicate the shear rates used for the comparison in (a). (c) Frequency sweeps corresponding to LVE envelopes in (a) and (b). The legend in (c) is common to the three subfigures.

position of the yielding strain γ_{max} varies only weakly with the shear rate for *Star35k-ZnCu-0.5*. Finally, in the steady-state regime, we observe a monotonic rise of the steady-state stress σ_{steady} with increasing $\dot{\gamma}$. This confirms smooth experiments and the absence of shear banding.[61] Despite the increase in σ_{steady}, a thinning behavior is observed in η_{steady}, which suggests that larger shear flow either forces the network to reorganize faster, i.e., decreases the lifetime of the stickers, or reduces the number density of associated supramolecular junctions, i.e., decreases their contribution to the elastic modulus.

Figure 7 compares the NLVE shear properties of the three MS networks based on *Star35k-ref* to evaluate the influence of the ion nature. Unlike the MS networks based on entangled stars (Pyromali et al.[37]), it was not possible to measure all three systems at a common temperature. For each network, temperatures that were too low caused early edge fracture due to brittle behavior, whereas temperatures that were too high resulted in excessive sample flow between the concentric cylinders of the CPP geometry due to the low viscosity.

Figure 7a compares the transient viscoelastic response of the three densely cross-linked networks at three representative shear rates. All systems exhibit shear hardening, but the effect is stronger for Cu^{2+}-containing networks. At the lowest shear rate (1 s^{-1}), the three curves lie close to their respective LVE envelopes (shown in Figure 7c), which are similar (τ_c on the same order of magnitude). Consequently, the steady-state viscosities follow the same trend as the terminal relaxation time (*Star35k-Cu-0.5* < *Star35k-Zn-0.5* < *Star35k-ZnCu-0.5*).

As the shear rate increases, the transient viscoelastic response of the three networks tends to merge, independent of ion identity or temperature. At 10 s^{-1}, the two single networks nearly overlap, while the dual-ion network requires a higher rate (56.2 s^{-1}) to approach the behavior of *Star35k-Zn-0.5*. No curve is shown for *Star35k-Cu-0.5* at this rate because the sample fractured at $\dot{\gamma}$ = 17.8 s^{-1}, again indicating the brittle character of densely cross-linked networks. A similar flow-dominated regime, where steady-state viscosity becomes independent of ion type, was previously reported by Pyromali et al.[37] for networks based on *Star250k-ref*.

This behavior is attributed to the fact that when flow dominates, chain relaxation and energy dissipation are not taking place anymore through the continuous 'natural' dissociation and association process of the stickers (characterized by a time $\tau_{sticker}$). As further discussed below, the flow rather forces the stickers to dissociate at shorter time, such that the network configuration can adapt to the deformation imposed by the flow. This leads to a flow-induced reduction of the sticker lifetime. A high shear rates, the sticker lifetime becomes so short that its value is dominated by the shear rate $\dot{\gamma}$, with no influence from the nature of the ions anymore.

In addition to the convergence of η_{steady}, Figure 7b shows a pronounced failure of the Cox–Merz rule as soon as the systems leave the LVR. Such deviations have been reported for supramolecular networks[27,29,35,62] and for branched polymers[59,63] and are attributed to the stretching of the molecular strands. The magnitude of the discrepancy here reflects the ability of the network strands to stretch and the ability of the stickers to continuously dissociate and reassociate, which is necessary for preserving the network integrity and avoiding the rupture of the sample. Hence, at high shear rates, the association/dissociation dynamics of the complexes still take place. However, the characteristic lifetime of the complexes, which is the same for the three systems, is fully governed by the flow and strand extensibility.

This proposition is further validated in Figure 8, which shows the overshoot strain γ_{max} as a function of the terminal

https://doi.org/10.1021/acs.macromol.6c00463
Macromolecules 2026, 59, 4636–4649

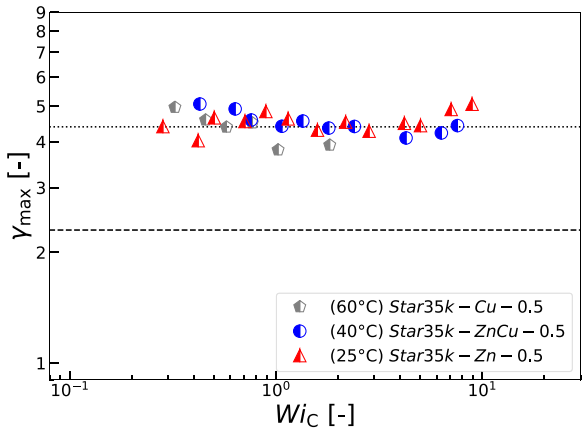

Figure 8. Strain at overshoot γ_{max} as a function of the terminal Weissenberg number Wi_c ($=\dot{\gamma}\tau_c$) for three MS networks build from *Star35k-ref*. The dashed line highlights the constant value of $\gamma_{max} = 2.3$ characteristic of a polymeric behavior during segmental orientation. The dotted line represents $\sqrt{M_{span}/M_k} \approx 4.4$.

Weissenberg number Wi_c for the three MS networks, which are compared in Figure 7. A classical polymer response (entangled linear chains, Doi & Edwards[64]) would display segment orientation with a constant $\gamma_{max} \approx 2.3$, followed by an increase at $Wi_R > 1$, due to chain stretching.[50,64] Our systems do not follow this trend: γ_{max} is essentially constant, independent of Wi_c, larger than 2.3, and unaffected by ionic composition. The strain accumulates until network strands reach a maximum extension, at which stickers are forced to dissociate.[26] This suggests that at high shear rates, the lifetime of a sticker should be well described by $\tau_{sticker,\ NLVE} \approx \gamma_{max}/\dot{\gamma}$, i.e., it should scale with $1/\dot{\gamma}$.

The shear-rate-independent γ_{max} indicates that network strands reach full extension regardless of ionic composition. To rationalize the observed constant value, we draw an analogy with the chain-dimension analysis of Fetters et al.[8,65] At equilibrium, network strands behave as random coils, with the distance between branching points proportional to $N_{strand}^{1/2} l_k$, where N_{strand} is the number of Kuhn segments per network strand and l_k the Kuhn length. In the fully extended state, the strand length scales as $N_{strand} l_k$. The resulting stretch ratio between the two states is

$$\lambda_{max} \propto \frac{N_{strand} l_k}{N_{strand}^{1/2} l_k} = N_{strand}^{1/2} \approx \gamma_{max} \tag{2}$$

For networks based on unentangled precursors, the mesh size is set by the molar mass between branching points, so

$$N_{strand} = \frac{M_{span}}{M_k} \tag{3}$$

where the Kuhn segment molar mass for P*n*BA is

$$M_k = M_0 \frac{l_k}{l_0} \tag{4}$$

with M_0 = 128.17 g/mol the monomer molar mass and l_0 = 2.55 Å the monomer step length (C2 backbone). The Kuhn length is given by

$$l_k = \frac{M_0}{l_0} \frac{\langle R^2 \rangle_0}{M} \tag{5}$$

and the unperturbed chain size per molar mass follows the empirical relation:[65]

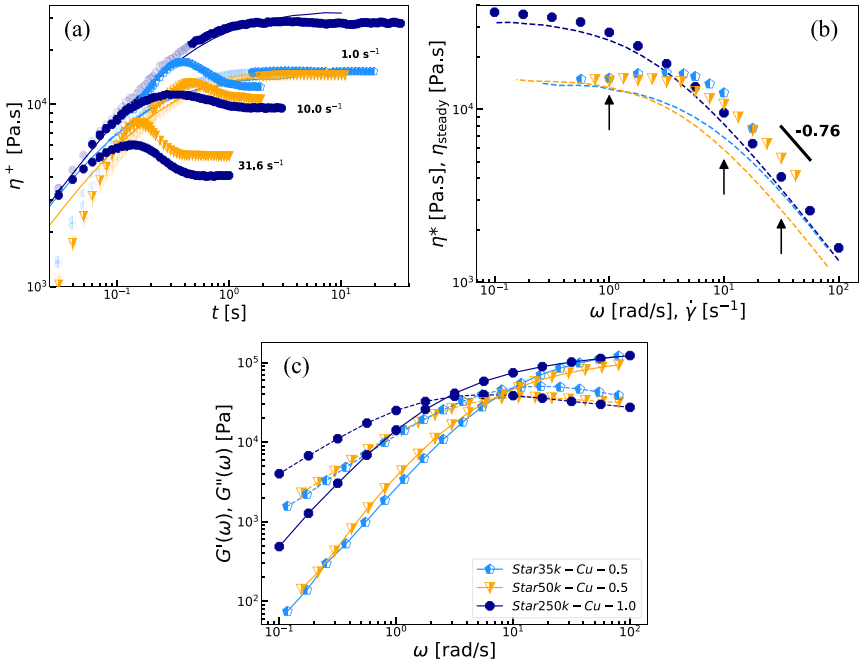

Figure 9. Influence of the precursor span. Comparison of the NLVE properties of three Cu^{2+}-based single networks at 60 °C. (a) Transient viscoelastic response at three different shear rates. Some data are shaded for clarity. LVE envelopes are indicated by straight lines. (b) Cox–Merz representation. Dashed lines correspond to the LVE envelopes. Black arrows indicate the shear rates used for the comparison in (a). (c) Frequency sweeps corresponding to LVE envelopes in (a) and (b). The legend in (c) is common to the three subfigures.

https://doi.org/10.1021/acs.macromol.6c00463
Macromolecules 2026, 59, 4636–4649

$$\frac{\langle R^2\rangle_0}{M} = \frac{1}{\rho N_A}\sqrt[3]{250\exp\left(\frac{T}{635}\right)\frac{G_N^0}{k_B T}} \quad (6)$$

With these relations, we obtain $l_k \approx 19.85$ Å and $M_k \approx 997$ g/mol, both approximated as temperature-independent. Using the M_{span} value employed in the LVE prediction for *Star35k-ref* (Figure 3), we find $\gamma_{max} \approx 4.39$ [-], shown as a horizontal dotted line in Figure 8, in excellent agreement with the data. Using M_e instead of M_{span} gives a similar value (4.24 [-]).

In the next section, we examine how key features (shear hardening, overshoot, Cox−Merz deviations, and γ_{max}) evolve when changing precursor size and thus mesh size and sticker density.

3.1.1.2. Influence of the Molar Mass of the Precursors. While the NLVE shear properties of networks based on entangled telechelic stars (*Star250k-ref*) were previously examined by Pyromali et al.,[37] the emphasis was mainly on the effect of sticker concentration and bond strength. More generally regarding telechelic networks, the literature lacks systematic studies investigating the influence of network strand size on both shear and elongational NLVE properties. Here, the availability of results with shorter precursors (*Star35k-ref* and *Star50k-ref*) enables us to assess how the precursor span affects the nonlinear response and to better dissociate the respective roles of stickers and entanglements under strong flows.

Figure 9 compares the NLVE behavior of three single MS networks containing Cu^{2+} (*Star35k-Cu-0.5*, *Star50k-Cu-0.5*, and *Star250k-Cu-1.0*) at 60 °C. Under equilibrium conditions, as shown in ref 22, sticker exchange dynamics are identical across systems (see also Figure 5 for the unentangled stars), and their LVE spectra are similar (Figure 9c, with τ_c of the same order of magnitude). Figure 9a presents their transient viscoelastic responses at three representative shear rates. At $\dot{\gamma} = 1\ s^{-1}$, the three curves lie close to their LVE envelopes. The steady-state viscosity of *Star250k-Cu-1.0* is higher than that of the two unentangled networks, whose transient viscoelastic responses nearly overlap.

Upon increasing the shear rate into the NLVR (e.g., $\dot{\gamma} = 10\ s^{-1}$), all curves deviate from their LVE envelopes but in distinct ways. The network based on entangled precursors deviates downward, whereas transient shear hardening occurs for the two unentangled systems. The upward deviation is stronger for *Star35k-Cu-0.5*, consistent with its shorter molecular span (and thus higher sticker density), which becomes stretched at lower shear rates. This also leads to a higher overshoot amplitude for shorter precursors (see the rate-dependent mechanical coherence, $\eta^+_{max}/\eta_{steady}$, in Figure S12).

The absence of transient shear hardening for *Star250k-Cu-1.0* indicates that before sticker dissociation begins the entanglement strands are not stretched, contrary to the network strands of the unentangled precursors. We attribute this difference to the fact that the arms can slide past one another, since the entanglements are not fixed cross-links. This sliding process allows the equilibration of the monomeric tension on a length scale defined by the network strands of mass M_{xx}, rather than limiting it to M_e, thus largely delaying the time at which entanglement segments start to stretch. This equilibration process at a larger length scale is also reflected in the shape of the overshoot, which is smoother and broader. Hence, while entanglements contribute similarly to stickers in the LVR by increasing the modulus, they behave differently in the NLVR: entanglements can slide and better adapt to the flow,[41] whereas stickers promote stress accumulation (see start-up elongation in the next section). Therefore, for *Star250k-Cu-1.0*, the yielding strain can no longer be attributed to sticker dissociation at full strand extension, and the broadness of the overshoot most probably results from a preliminary equilibration at the length scale of entanglement strands before eventually reaching full strand extension. Further development of theoretical pictures such as the shear slit model[50] would be beneficial to rationalize such overshoot broadness.

Figure 9b compares their steady-state viscosity to their linear complex viscosity. It is observed that all networks exhibit shear thinning. However, the steady-state behavior strongly depends on precursor span. For entangled precursors, Cox−Merz deviations appear at low shear rates (more pronounced at 40 °C for *Star250k-Cu-1.0*,[37] not shown) but the rule is recovered at high shear rates, where sticker effects become negligible.[37] The opposite trend is observed for unentangled networks (*Star35k-Cu-0.5* and *Star50k-Cu-0.5*): their steady-state viscosity deviates strongly upward from the LVE envelope and never reaches it again. Instead, η_{steady} evolves 'in parallel' with the LVE envelope and with the values of *Star250k-Cu-1.0* (slope ≈ -0.76). At high shear rates, η_{steady} becomes independent of bond strength for a given precursor, but remains sensitive to precursor span and thus to sticker density and maximum stretch ratio. Higher sticker density promotes more recombination events, leading to a permanent stretch and a higher steady-state viscosity. Moreover, for sample *Star250k-Cu-1.0*, the validity of the Cox Merz rule at high shear rates suggests that the dissipative units are still the entanglement segments, with the latter remaining unstretched. The high molar mass of the network strands (M_{XX} = 125 kg/mol, number-average) ensures that the chain does not reach its maximum stretch level, λ_{max}, estimated to 11.7, before the dissociation of the stickers.

In Figure 8, we showed that for the shortest precursors, γ_{max} is independent of bond strength and is instead set by the full extension of the network strands. Figure 10 shows that MS networks based on longer precursors (*Star50k-ref* and *Star250k-ref*) may still display an approximately constant γ_{max}. However, this value is no longer controlled by full strand extension, especially in the case of the entangled precursors. At a low shear rate, it is observed that γ_{max} becomes rate-dependent when sticker exchange is too fast relative to the time at which network strands start being stretched (e.g., *Star50k-Zn-0.5* at 25 °C in Figure 10a; *Star250k-Zn-1.0* at 40 °C and *Star250k-Cu-1.0* at 60 °C in Figure 10b).

At higher shear rates, when sticker lifetimes are sufficiently long compared to the flow (as for *Star50k-Cu-0.5* at 60 °C and *Star50k-Zn-0.5* at 20 °C in Figure 10a and *Star250k-ZnCu-1.0* and *Star250k-Cu-1.0* at 40 °C in Figure 10b), the networks exhibit the same qualitative behavior as in Figure 8: γ_{max} remains constant and exceeds 2.3. Yet the constant value is no longer consistent with eq 2 (dotted lines: $\sqrt{M_{span}/M_k} \approx 5.7$ in Figure 10a and 11.7 in Figure 10b). Instead, it lies closer to $\sqrt{M_e/M_k} \approx 4.2$ (solid lines), with slightly higher values for the larger precursors (Figure 10b). This value further suggests a preliminary equilibration of the tension at the length scale of the entanglement strands before propagating to the full strand length.

https://doi.org/10.1021/acs.macromol.6c00463
Macromolecules 2026, 59, 4636−4649

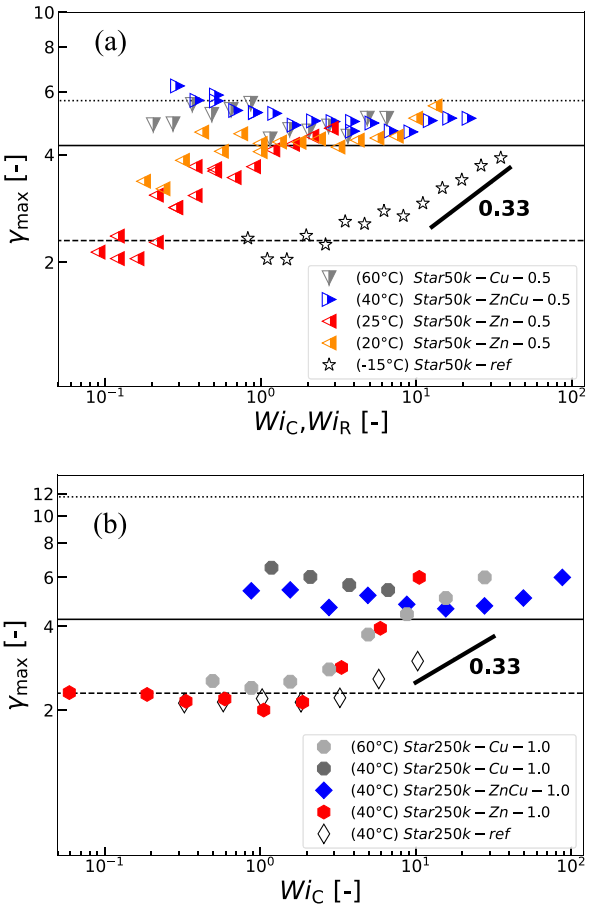

Figure 10. Strain at overshoot γ_{max} as a function of the terminal Weissenberg number $Wi_c = \dot{\gamma}\tau_c$ (or $Wi_R = \dot{\gamma}\tau_R$ for *Star50k-ref*). (a) *Star50k-ref* and related MS networks. (b) *Star250k-ref* and related MS networks. Measurement temperatures are indicated in legend. The dashed line highlights the constant value of γ_{max}= 2.3 characteristic of a polymeric behavior during segmental orientation. The straight line represents $\sqrt{M_e/M_k} \approx 4.2$. The dotted line represents $\sqrt{M_{span}/M_k} \approx 5.7$ with *Star50k-ref* (a) and ≈11.7 with *Star250k-ref* (b).

In Figure 10, we also observe that the precursors behave as expected: γ_{max} is constant (≈2.3, dashed lines) at low Weissenberg numbers and increases with a slope close to 0.33 under stronger flows.

3.2.3. Nonlinear Viscoelasticity: Start-Up Elongation. To further assess the role of entanglements in sticker recombination and in the brittle- or ductile-like response of SPNs, we performed start-up extensional experiments. Figure 11 compares the stress–strain curves at 40 °C for *Star50k-Cu-0.5* and *Star250k-Cu-1.0*, for which the main varying parameter is the network strand length (and thus the sticker density).

Both networks exhibit pronounced strain hardening. A clear upward deviation of $\eta_E^+(t)$ curves from the respective LVE envelopes can be observed in Figure S14. Hardening is observed at a smaller Hencky strain for *Star50k-Cu-0.5* (orange), likely because shorter strands become stretched more readily. With larger precursors (in blue), entanglements can first slide before the network strands start to stretch,[66] at a higher Hencky strain.

Although both samples exhibit hardening, their failure behavior differs markedly. For the network based on unentangled precursors (*Star50k-Cu-0.5*), the filament ruptures for all investigated strain rates (black crossed symbols),

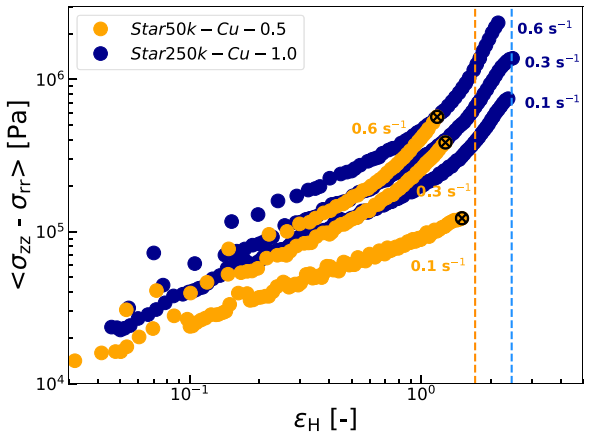

Figure 11. Influence of M_{span}. Stress–strain curves for *Star50k-Cu-0.5* and *Star250k-Cu-1.0* at 40 °C. The experimental Hencky strain rates $\dot{\epsilon}_H$ for the two samples are indicated on the graph. Black crossed symbols indicate filament rupture points. Vertical dashed lines are calculated values for $\epsilon_{H,max} = \ln N_{strand}^{1/2}$.

whereas the network formed from entangled stars (*Star250k-Cu-1.0*) could be extended up to the instrumental limit. This contrast highlights an additional dissipation pathway in entangled systems. To rationalize filament rupture, we compare the measured strains with the maximum strand extension $\epsilon_{H,max} = \ln N_{strand}^{1/2}$, following Wu et al.[8] (and analogously to eq 2 in shear). These values are indicated by dashed vertical lines in Figure 11.

For the entangled network (blue curves), the maximum stress occurs close to $\epsilon_{H,max}$ (≈2.5), independent of the strain rate. For larger strains, filament rupture is avoided as entanglements maintain the sample integrity and dissociated strands must first disentangle.[41] In addition, the long precursor relaxation time possibly allows Cu^{2+}/tpy stickers to recombine before full arm retraction, further delaying the failure.

In contrast, the network based on shorter unentangled precursors ruptures at all rates. Here, precursor relaxation is fast (Rouse-like), so once stickers dissociate, they are unlikely to recombine. At the lowest rate (0.1 s^{-1}), rupture occurs near $\epsilon_{H,max}$(≈1.7), whereas at higher rates (0.3 and 0.6 s^{-1}), failure occurs at lower strains and higher stresses. Strong strain hardening likely induces stress concentrations that promote premature sticker dissociation. Moreover, the brittle failure suggests that under extensional flow, sticker recombination does not occur for these systems.[25]

In Figure 12, the elongation properties of the two networks built from unentangled or barely entangled precursors are compared. It is seen that strain hardening (see also $\eta_E^+(t)$ curves in Figure S15), followed by filament rupture, is taking place at shorter deformation for *Star35k-Cu-0.5*, compared to *Star50k-Cu-0.5*. This comparison highlights the large influence of the maximum stretchability of the sample, λ_{max}, on the strain hardening properties of the networks: at the large Hencky strain rate, the stress curves deviate upward from a linear dependence on ε_H and the network breaks shortly after, suggesting that the non-Gaussian regime of deformation is reached. The limit of the Gaussian regime directly depends on the ability of the network strand to stretch, i.e., on its number of Kuhn segments.

As already mentioned, the sharp rupture of these networks is attributed to the inability of the dissociated stickers to create new bonds. Once a supramolecular junction is broken, the

https://doi.org/10.1021/acs.macromol.6c00463
Macromolecules 2026, 59, 4636–4649

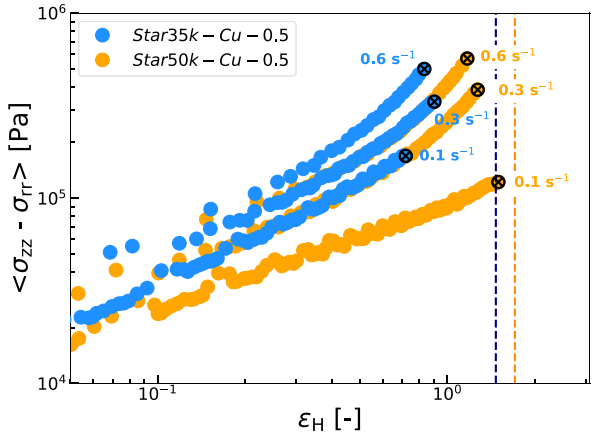

Figure 12. Stress–strain curves for *Star35k-Cu-0.5* and *Star50k-Cu-0.5* at 40 °C. The experimental Hencky strain rates $\dot{\epsilon}_H$ for the two samples are indicated on the graph. Black crossed symbols indicate filament rupture points. Vertical dashed lines are calculated values for $\epsilon_{H,max} = \ln N_{strand}^{1/2}$.

retraction of the free star arms is too fast to allow the chain ends the possibility of creating a new supramolecular junction. To delay the rupture of the samples, weaker bonds, characterized by a shorter lifetime, should be introduced into the nework. Indeed, since the weaker bonds dissociate at shorter time, the corresponding network strands do not have time to stretch and their probability to reassociate should therefore be higher.[40]

4. CONCLUSIONS

We investigated the nonlinear viscoelastic properties, both in shear and in elongation, of telechelic metallosupramolecular polymer networks in the melt state. Nonlinear shear measurements were performed using cone-partitioned-plate rheometry, while elongation measurements were performed using filament stretching rheometry. The (non)linear properties were studied by systematically varying strand length (unentangled, barely entangled, and well-entangled star precursors) or bond strength (Zn^{2+}, Cu^{2+}, and blends).

In nonlinear shear, for densely cross-linked networks (based on unentangled and barely entangled precursors), we showed that, unlike networks based on entangled precursors, pronounced transient shear hardening was observed and attributed to arm stretching, with $\eta^+(t)$ increasing well above the LVE envelope up to a maximum dictated by the dissociation of the stickers, before decreasing toward its steady-state value. Stress–strain curves revealed an elastic deformation with a slope of 1 for most of the shear rates, except for the highest ones at which an upward deviation from this slope was observed, suggesting that network strands become stretched. Regarding the steady-state regime, a strong failure of the Cox–Merz rule was observed for these densely cross-linked networks, unlike networks based on entangled telechelic stars. This was interpreted as the result of frequent dissociation/reassociation events for the stickers leading to a permanent stretching of star arms, in average.

A shear-rate-independent deformation at the stress-overshoot maximum γ_{max} was observed for the networks based on the shortest, unentangled stars no matter the bond strength. We therefore concluded to a strain-induced sticker dissociation, with the sticker lifetime scaling with $1/\dot{\gamma}$. This flow-induced reduction of the sticker lifetime was further supported by the merging transient and steady-state viscoelastic responses of unentangled networks at high shear rates, regardless of the ions involved or the temperature. For these networks based on unentangled stars, the value of γ_{max} was well-predicted by $N_{strand}^{1/2}$ (the maximum stretching ratio of a network strand), while for networks based on the entangled stars at intermediate shear rates, γ_{max} was found to rather correspond to $N_e^{1/2}$. In elongation, we observed that networks formed from short stars ruptured at a Hencky strain slightly smaller than the maximum stretching ratio, $\epsilon_{H,max} = \ln N_{strand}^{1/2}$, demonstrating again the importance of this ratio.

On the contrary, for the well-entangled networks, the filament did not rupture during the elongation tests. Entanglements no longer act as effective cross-linking points in the nonlinear regime. Instead, longer arms allow chain sliding. This constitutes an additional energy dissipation pathway, reducing strain hardening and postponing the strain at which network strands become stretched. Densely cross-linked networks are therefore stiffer but more brittle, while the presence of entanglements in long arms makes the networks tougher. To combine stiffness and toughness, dual networks based on unentangled telechelic stars appear as a promising strategy.

■ ASSOCIATED CONTENT

Supporting Information

The Supporting Information is available free of charge at https://pubs.acs.org/doi/10.1021/acs.macromol.6c00463.

Polymerization protocol, deconvolution of the chromatogram obtained by GPC; frequency sweeps and the shear rate range; transient viscoelastic responses; rate-dependent fractional viscosity overshoot; and the definition of all of the acronyms and parameters used in the paper (PDF)

■ AUTHOR INFORMATION

Corresponding Author

Pierrot de Wergifosse – *Bio- and Soft Matter (BSMA), Institute of Condensed Matter and Nanosciences, Université catholique de Louvain, B-1348 Louvain-La-Neuve, Belgium;* orcid.org/0009-0000-0912-2168;
Email: pierrot.dewergifosse@uclouvain.be

Authors

Maxime Dalne – *Bio- and Soft Matter (BSMA), Institute of Condensed Matter and Nanosciences, Université catholique de Louvain, B-1348 Louvain-La-Neuve, Belgium*

Alvaro Quinteros-Sedano – *Bio- and Soft Matter (BSMA), Institute of Condensed Matter and Nanosciences, Université catholique de Louvain, B-1348 Louvain-La-Neuve, Belgium*

Evelyne van Ruymbeke – *Bio- and Soft Matter (BSMA), Institute of Condensed Matter and Nanosciences, Université catholique de Louvain, B-1348 Louvain-La-Neuve, Belgium;* orcid.org/0000-0001-7633-0194

Complete contact information is available at: https://pubs.acs.org/10.1021/acs.macromol.6c00463

Notes

The authors declare no competing financial interest.

https://doi.org/10.1021/acs.macromol.6c00463
Macromolecules 2026, 59, 4636–4649

■ ACKNOWLEDGMENTS

We thank Prof. Dimitris Vlassopoulos and his group for helping us gathering nonlinear shear experimental data: Dr. Christina Pyromali for sharing her data on entangled stars and Dr. Jiaqi Zhang for measuring the shortest star precursor. We thank Dr. Yanzhao Li for performing nonlinear elongational experiments on the entangled stars. E.V.R. is a Senior Research Associate of the FRS-FNRS. P.D.W. is a Research Fellow (ASP) of the FRS-FNRS. We thank the Excellence of Science programme (grant EOS 40007519) from the FWO and F.R.S.-FNRS for financial support.

■ REFERENCES

(1) Guo, M.; Pitet, L. M.; Wyss, H. M.; Vos, M.; Dankers, P. Y. W.; Meijer, E. W. Tough Stimuli-Responsive Supramolecular Hydrogels with Hydrogen-Bonding Network Junctions. *J. Am. Chem. Soc.* **2014**, *136* (19), 6969−6977.

(2) Song, P.; Wang, H. High-Performance Polymeric Materials through Hydrogen-Bond Cross-Linking. *Adv. Mater.* **2020**, *32* (18), 1901244.

(3) Cordier, P.; Tournilhac, F.; Soulié-Ziakovic, C.; Leibler, L. Self-healing and thermoreversible rubber from supramolecular assembly. *Nature* **2008**, *451* (7181), 977−980.

(4) Hawke, L.; Ahmadi, M.; Goldansaz, H.; van Ruymbeke, E. Viscoelastic properties of linear associating poly(n-butyl acrylate) chains. *J. Rheol.* **2016**, *60* (2), 297−310.

(5) Shi, L.; Ding, P.; Wang, Y.; Zhang, Y.; Ossipov, D.; Hilborn, J. Self-Healing Polymeric Hydrogel Formed by Metal−Ligand Coordination Assembly: Design, Fabrication, and Biomedical Applications. *Macromol. Rapid Commun.* **2019**, *40* (7), 1800837.

(6) Winter, A.; Schubert, U. S. Synthesis and characterization of metallo-supramolecular polymers. *Chem. Soc. Rev.* **2016**, *45* (19), 5311−5357.

(7) Tang, Z.; Huang, J.; Guo, B.; Zhang, L.; Liu, F. Bioinspired Engineering of Sacrificial Metal−Ligand Bonds into Elastomers with Supramechanical Performance and Adaptive Recovery. *Macromolecules* **2016**, *49* (5), 1781−1789.

(8) Wu, S.; Cao, X.; Zhang, Z.; Chen, Q.; Matsumiya, Y.; Watanabe, H. Molecular Design of Highly Stretchable Ionomers. *Macromolecules* **2018**, *51* (12), 4735−4746.

(9) Chen, Q.; Tudryn, G.; Colby, R. Ionomer dynamics and the sticky Rouse model. *J. Rheol.* **2013**, *57*, 1441−1462.

(10) Zhang, Z.; Chen, Q.; Colby, R. H. Dynamics of associative polymers. *Soft Matter* **2018**, *14* (16), 2961−2977.

(11) Shabbir, A.; Huang, Q.; Chen, Q.; Colby, R. H.; Alvarez, N. J.; Hassager, O. Brittle fracture in associative polymers: The case of ionomer melts. *Soft Matter* **2016**, *12* (36), 7606−7612.

(12) van Ruymbeke, E. Preface: Special Issue on Associating Polymers. *J. Rheol.* **2017**, *61* (6), 1099−1102.

(13) Cerdan, K.; Thys, M.; Costa Cornellà, A.; Demir, F.; Norvez, S.; Vendamme, R.; Van den Brande, N.; Van Puyvelde, P.; Brancart, J. Sustainability of self-healing polymers: A holistic perspective towards circularity in polymer networks. *Prog. Polym. Sci.* **2024**, *152*, No. 101816.

(14) Niu, W.; Li, Z.; Liang, F.; Zhang, H.; Liu, X. Ultrastable, Superrobust, and Recyclable Supramolecular Polymer Networks. *Angew. Chem., Int. Ed.* **2024**, *63* (10), No. e202318434.

(15) Sun, J.-Y.; Zhao, X.; Illeperuma, W. R. K.; Chaudhuri, O.; Oh, K. H.; Mooney, D. J.; Vlassak, J. J.; Suo, Z. Highly stretchable and tough hydrogels. *Nature* **2012**, *489* (7414), 133−136.

(16) Zhao, X. Multi-scale multi-mechanism design of tough hydrogels: Building dissipation into stretchy networks. *Soft Matter* **2014**, *10* (5), 672−687.

(17) Skrzeszewska, P. J.; Sprakel, J.; de Wolf, F. A.; Fokkink, R.; Cohen Stuart, M. A.; van der Gucht, J. Fracture and Self-Healing in a Well-Defined Self-Assembled Polymer Network. *Macromolecules* **2010**, *43* (7), 3542−3548.

(18) Burattini, S.; Colquhoun, H. M.; Fox, J. D.; Friedmann, D.; Greenland, B. W.; Harris, P. J. F.; Hayes, W.; Mackay, M. E.; Rowan, S. J. A self-repairing, supramolecular polymer system: Healability as a consequence of donor−acceptor $\pi-\pi$ stacking interactions. *Chem. Commun.* **2009**, *44*, 6717−6719.

(19) Wu, S.; Chen, Q. Advances and New Opportunities in the Rheology of Physically and Chemically Reversible Polymers. *Macromolecules* **2022**, *55* (3), 697−714.

(20) Rubinstein, M.; Semenov, A. N. Dynamics of Entangled Solutions of Associating Polymers. *Macromolecules* **2001**, *34* (4), 1058−1068.

(21) Boudara, V. A. H.; Read, D. J. Stochastic and preaveraged nonlinear rheology models for entangled telechelic star polymers. *J. Rheol.* **2017**, *61* (2), 339−362.

(22) de Wergifosse, P.; Lyons, R.; Fustin, C.-A.; van Ruymbeke, E. Viscoelastic Properties of Metallo-Supramolecular Networks: Relationship Between Sticker/Entanglement Dynamics and Terminal Relaxation. *Macromolecules* **2025**, *58* (1), 222−239.

(23) Snijkers, F.; Vlassopoulos, D. Cone-Partitioned-Plate Geometry for the ARES Rheometer with Temperature Control. *J. Rheol.* **2011**, *55* (6), 1167−1186.

(24) Bach, A.; Rasmussen, H. K. Hassager, O; Extensional viscosity for polymer melts measured in the filament stretching rheometer. *J. Rheol.* **2003**, *47* (2), 429−441.

(25) Amin, D.; Wang, Z. Nonlinear rheology and dynamics of supramolecular polymer networks formed by associative telechelic chains under shear and extensional flows. *J. Rheol.* **2020**, *64* (3), 581−600.

(26) Berret, J.-F.; Séréro, Y. Evidence of Shear-Induced Fluid Fracture in Telechelic Polymer Networks. *Phys. Rev. Lett.* **2001**, *87* (4), No. 048303.

(27) Suzuki, S.; Uneyama, T.; Inoue, T.; Watanabe, H. Nonlinear Rheology of Telechelic Associative Polymer Networks: Shear Thickening and Thinning Behavior of Hydrophobically Modified Ethoxylated Urethane (HEUR) in Aqueous Solution. *Macromolecules* **2012**, *45* (2), 888−898.

(28) Tripathi, A.; Tam, K. C.; McKinley, G. H. Rheology and Dynamics of Associative Polymers in Shear and Extension: Theory and Experiments. *Macromolecules* **2006**, *39* (5), 1981−1999.

(29) Park, G. W.; Ianniruberto, G. A new stochastic simulation for the rheology of telechelic associating polymers. *J. Rheol.* **2017**, *61* (6), 1293−1305.

(30) Shabbir, A.; Goldansaz, H.; Hassager, O.; van Ruymbeke, E.; Alvarez, N. J. Effect of Hydrogen Bonding on Linear and Nonlinear Rheology of Entangled Polymer Melts. *Macromolecules* **2015**, *48* (16), 5988−5996.

(31) Shabbir, A.; Huang, Q.; Baeza, G. P.; Vlassopoulos, D.; Chen, Q.; Colby, R. H.; Alvarez, N. J.; Hassager, O. Nonlinear shear and uniaxial extensional rheology of polyether-ester-sulfonate copolymer ionomer melts. *J. Rheol.* **2017**, *61* (6), 1279−1289.

(32) Stadler, F. J.; Still, T.; Fytas, G.; Bailly, C. Elongational Rheology and Brillouin Light Scattering of Entangled Telechelic Polybutadiene Based Temporary Networks. *Macromolecules* **2010**, *43* (18), 7771−7778.

(33) Cox, W. P.; Merz, E. H. Correlation of dynamic and steady flow viscosities. *J. Polym. Sci.* **1958**, *28* (118), 619−622.

(34) Snijkers, F.; Ratkanthwar, K.; Vlassopoulos, D.; Hadjichristidis, N. Viscoelasticity, Nonlinear Shear Start-up, and Relaxation of Entangled Star Polymers. *Macromolecules* **2013**, *46* (14), 5702−5713.

(35) Pellens, L.; Gamez Corrales, R.; Mewis, J. General nonlinear rheological behavior of associative polymers. *J. Rheol.* **2004**, *48* (2), 379−393.

(36) Séréro, Y.; Jacobsen, V.; Berret, J.-F.; May, R. Evidence of Nonlinear Chain Stretching in the Rheology of Transient Networks. *Macromolecules* **2000**, *33* (5), 1841−1847.

(37) Pyromali, C.; Li, Y.; Zhuge, F.; Fustin, C.-A.; van Ruymbeke, E.; Vlassopoulos, D. Nonlinear shear rheology of single and double dynamics metal-ligand networks. *J. Rheol.* **2022**, *66* (6), 1223−1235.

https://doi.org/10.1021/acs.macromol.6c00463
Macromolecules 2026, 59, 4636−4649

(38) Yan, T.; Schröter, K.; Herbst, F.; Binder, W. H.; Thurn-Albrecht, T. What Controls the Structure and the Linear and Nonlinear Rheological Properties of Dense, Dynamic Supramolecular Polymer Networks? *Macromolecules* **2017**, *50* (7), 2973−2985.
(39) Arora, S.; Shabbir, A.; Hassager, O.; Ligoure, C.; Ramos, L. Brittle fracture of polymer transient networks. *J. Rheol.* **2017**, *61* (6), 1267−1275.
(40) Liu, S.; Cao, X.; Huang, C.; Weiss, R. A.; Zhang, Z.; Chen, Q. Brittle-to-Ductile Transition of Sulfonated Polystyrene Ionomers. *ACS Macro Lett.* **2021**, *10* (4), 503−509.
(41) Kim, J.; Zhang, G.; Shi, M.; Suo, Z. Fracture, fatigue, and friction of polymers in which entanglements greatly outnumber cross-links. *Science* **2021**, *374* (6564), 212−216.
(42) Li, Y.; Pyromali, C.; Zhuge, F.; Fustin, C.-A.; Gohy, J.-F.; van Ruymbeke, E. Dynamics of entangled metallosupramolecular polymer networks combining stickers with different lifetimes. *J. Rheol.* **2022**, *66*, 1203.
(43) Zhuge, F.; Brassinne, J.; Fustin, C.-A.; van Ruymbeke, E.; Gohy, J.-F. Synthesis and Rheology of Bulk Metallo-Supramolecular Polymers from Telechelic Entangled Precursors. *Macromolecules* **2017**, *50* (13), 5165−5175.
(44) Ghiassinejad, S.; Mortensen, K.; Rostamitabar, M.; Malineni, J.; Fustin, C.-A.; van Ruymbeke, E. Dynamics and Structure of Metallo-supramolecular Polymers Based on Short Telechelic Precursors. *Macromolecules* **2021**, *54* (13), 6400−6416.
(45) Román Marín, J. M.; Huusom, J. K.; Alvarez, N. J.; Huang, Q.; Rasmussen, H. K.; Bach, A.; Skov, A. L.; Hassager, O. A control scheme for filament stretching rheometers with application to polymer melts. *J. Non-Newtonian Fluid Mech.* **2013**, *194*, 14−22.
(46) Rasmussen, H. K.; Bejenariu, A. G.; Hassager, O.; Auhl, D. Experimental evaluation of the pure configurational stress assumption in the flow dynamics of entangled polymer melts. *J. Rheol.* **2010**, *54* (6), 1325−1336.
(47) van Ruymbeke, E.; Muliawan, E. B.; Vlassopoulos, D.; Gao, H.; Matyjaszewski, K. Melt rheology of star polymers with large number of small arms, prepared by crosslinking poly(*n*-butyl acrylate) macromonomers via ATRP. *Eur. Polym. J.* **2011**, *47* (4), 746−751.
(48) Rouse, P. E., Jr. A Theory of the Linear Viscoelastic Properties of Dilute Solutions of Coiling Polymers. *J. Chem. Phys.* **1953**, *21* (7), 1272−1280.
(49) Gleissle, W. *Two Simple Time-Shear Rate Relations Combining Viscosity and First Normal Stress Coefficient in the Linear and Non-Linear Flow Range*; Springer: Boston, MA, 1980.
(50) Dalne, M.; Costanzo, S.; Peponaki, K.; Jiang, N.; Alexandris, S.; Grizzuti, N.; Vlassopoulos, D.; Rubinstein, M.; van Ruymbeke, E. Nonlinear Shear Rheology of Unentangled Polymer Melts. *Macromolecules* **2025**, *58* (14), 7062−7083.
(51) Costanzo, S.; Huang, Q.; Ianniruberto, G.; Marrucci, G.; Hassager, O.; Vlassopoulos, D. Shear and Extensional Rheology of Polystyrene Melts and Solutions with the Same Number of Entanglements. *Macromolecules* **2016**, *49* (10), 3925−3935.
(52) Ianniello, V.; Costanzo, S. Linear and nonlinear shear rheology of nearly unentangled H-polymer melts and solutions. *Rheol. Acta* **2022**, *61* (10), 667−679.
(53) Huang, Q.; Costanzo, S.; Das, C.; Vlassopoulos, D. Stress growth and relaxation of dendritically branched macromolecules in shear and uniaxial extension. *J. Rheol.* **2017**, *61* (1), 35−47.
(54) Snijkers, F.; Lee, H.; Chang, T.; Das, C.; Vlassopoulos, D. Start-up shear flow of a well-characterized entangled H-polymer. *Eur. Polym. J.* **2024**, *206*, No. 112806.
(55) Snijkers, F.; Vlassopoulos, D.; Lee, H.; Yang, J.; Chang, T.; Driva, P.; Hadjichristidis, N. Start-up and relaxation of well-characterized comb polymers in simple shear. *J. Rheol.* **2013**, *57* (4), 1079−1100.
(56) Tezel, A. K.; Oberhauser, J. P.; Graham, R. S.; Jagannathan, K.; McLeish, T. C. B.; Leal, L. G. The nonlinear response of entangled star polymers to startup of shear flow. *J. Rheol.* **2009**, *53* (5), 1193−1214.
(57) Li, B.; Vlassopoulos, D. Undershoot Recovery in Polystyrene Melts: Effects of Annealing on Repeated Shear Startup. *J. Phys. Chem. B* **2026**, *130* (1), 533−546.
(58) Rathinaraj, J.D. J.; Keshavarz, B.; McKinley, G. H. Why the Cox−Merz rule and Gleissle mirror relation work: A quantitative analysis using the Wagner integral framework with a fractional Maxwell kernel. *Phys. Fluids* **2022**, *34* (3), No. 033106.
(59) Snijkers, F.; Vlassopoulos, D. Appraisal of the Cox-Merz rule for well-characterized entangled linear and branched polymers. *Rheol. Acta* **2014**, *53* (12), 935−946.
(60) Ianniruberto, G.; Marrucci, G. Entangled Melts of Branched PS Behave Like Linear PS in the Steady State of Fast Elongational Flows. *Macromolecules* **2013**, *46* (1), 267−275.
(61) Fielding, S. M.; Cates, M. E.; Sollich, P. Shear banding, aging and noise dynamics in soft glassy materials. *Soft Matter* **2009**, *5* (12), 2378−2382.
(62) Parisi, D.; Ditillo, C. D.; Han, A.; Lindberg, S.; Hamersky, M. W.; Colby, R. H. Rheological investigation on the associative properties of poly(vinyl alcohol) solutions. *J. Rheol.* **2022**, *66* (6), 1141−1150.
(63) Schußmann, M. G.; Song, H. Y.; Hyun, K.; Wilhelm, M.; Hirschberg, V. Double stress overshoot in startup shear flow and failure of Cox−Merz rule of pom-pom polymers. *Phys. Fluids* **2025**, *37* (1), No. 013109.
(64) Doi, M.; Edwards, S. F. *The Theory of Polymer Dynamics*; Oxford University Press, 1988.
(65) Fetters, L. J.; Lohse, D. J.; Colby, R. H. Chain Dimensions and Entanglement Spacings. In *Physical Properties of Polymers Handbook*; Mark, J. E., Ed.; Springer, 2007; pp 447−454.
(66) Wang, S.-Q. *Nonlinear Polymer Rheology: Macroscopic Phenomenology and Molecular Foundation*; John Wiley &Sons, 2018.

https://doi.org/10.1021/acs.macromol.6c00463
Macromolecules 2026, 59, 4636−4649